ACS Sustainable Chemistry & Engineering

pubs.acs.org/journal/ascecg

Research Article

Thermoresponsive Smart Gating Wood Membranes

Yong Ding, Guido Panzarasa, Sandro Stucki, Ingo Burgert,* and Tobias Keplinger

Cite This: ACS Sustainable Chem. Eng. 2022, 10, 5517−5525

Read Online

ACCESS | Metrics & More | Article Recommendations | Supporting Information

ABSTRACT: Smart membranes that can open and/or close their pores in a controlled manner by external stimuli possess potential in various applications, such as water flow manipulation, indoor climate regulation, and sensing. The design of smart gating membranes with high flux, immediate response, and mechanical robustness is still an open challenge, limiting their versatility and practical applicability. Inspired by the controlled opening and closure of plant stomata, we have developed a smart gating wood membrane, taking advantage of the unique wood scaffold with its hierarchical porous structure to carry thermoresponsive hydrogel gates. Laser drilling was applied to cut channels in the wood scaffold with well-aligned pores to incorporate the smart gating membranes. In situ polymerization of poly(N-isopropylacrylamide) above its lower critical solution temperature inside the channels resulted in a hydrogel with a heterogeneous microstructure acting as a thermoresponsive gate. The wood-based smart gating membranes exhibited reversible and stable pore opening/closing under heating/cooling stimuli. The achieved rapid response and feasibility of scale-up open the venue for various practical applications. In this work, we demonstrated their potential for indoor light regulation and as a water flow manipulator.

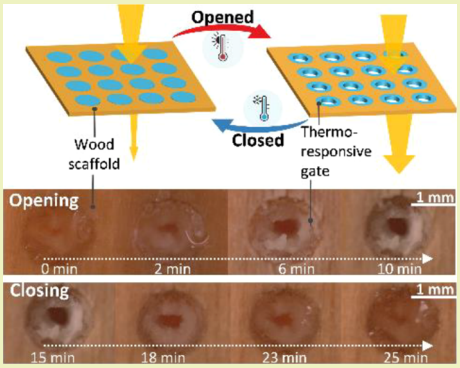

KEYWORDS: *smart gating membrane, stimuli responsive, wood, hydrogel, bioinspired, biobased composites*

INTRODUCTION

Smart gating membranes can open and/or close their pores in a controlled manner upon external stimulation, such as changes in temperature, light, pH, mechanical stress, and electric or magnetic fields. These smart gating membranes have gained increasing attention, thanks to simple operation, low energy demand, and no need for dedicated accessories compared to conventional actuator systems.[1−3] Despite many recent efforts, developing smart gating membranes with both excellent gating performance (e.g., high flux and fast response time) and technical feasibility (e.g., with sufficient mechanical robustness and of simple, environmentally friendly fabrication) remains an open challenge.

Inspiration from nature represents one possible way to overcome this challenge. One example are plant stomata (Figure 1a).[4] Stomata are microrespirational pores composed of two symmetric guard cells, which are tightly embedded in epidermal cells. To open, the guard cells take in ions through their membranes, which results in an influx of water across the guard cell membrane. As the volume of the guard cells increase, they "inflate" into two kidney-bean-like shapes because of an unequal thickness of cell walls and their cellulose microfibril orientation. As they expand in a preferential direction, they reveal the stomata opening in the center of the two guard cells for gas exchange. The stomata's pores close in the opposite manner.

Inspired by the structure of plant stomata, artificial smart gating membranes have been developed by chemically/physically incorporating stimuli-responsive materials as functional gates into porous membranes.[1,5] In response to environmental stimuli, such as temperature changes, these functional gates undergo a conformational switch, adjusting the pore sizes and thus regulating permeability.[6] For example, Du et al. prepared nanocellulose sponge-poly(N-isopropylacrylamide) (PNIPAM) composites for thermoresponsive water flow manipulation.[2] The volume change of the PNIPAM hydrogel at a lower critical solution temperature (LCST) enabled its use as a thermoresponsive polymer as it is well-studied, easily synthesized, and of low cost.

However, most commonly employed porous substrates, prepared by chemical etching or freeze-drying, have inherent limits such as irregular pore sizes, lack of pore order/orientation, weak mechanical properties and difficult scale-up fabrication processes. In addition, current smart gating membranes still suffer from low flux, poor responsiveness, or stable actuation, which severely impede their practical application.

Therefore, we propose here the utilization of wood as the gate bearing substrate. Wood is a porous material and

Received: January 6, 2022
Revised: April 1, 2022
Published: April 20, 2022

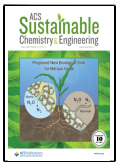

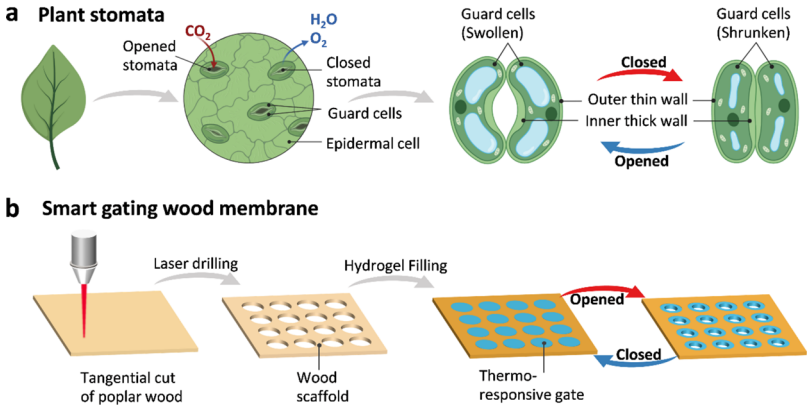

Figure 1. Schematic representation of plant stomata as the source of inspiration and developed smart gating wood membrane. (a) Illustration of plant stomata composed of two symmetric guard cells embedded in epidermal cells. The stomata open when guard cells swell and close when guard cells shrink. (b) Developed fabrication process for the thermoresponsive smart gating wood membrane. First, channel arrays were drilled by laser beam. Then, the 3D wood scaffold was pretreated with methacrylic anhydride. N-isopropylacrylamide was polymerized in situ to fill the pores with thermoresponsive hydrogels. The thermoresponsive smart gating wood membrane pores close below LCST and open above LCST of poly(N-isopropylacrylamide).

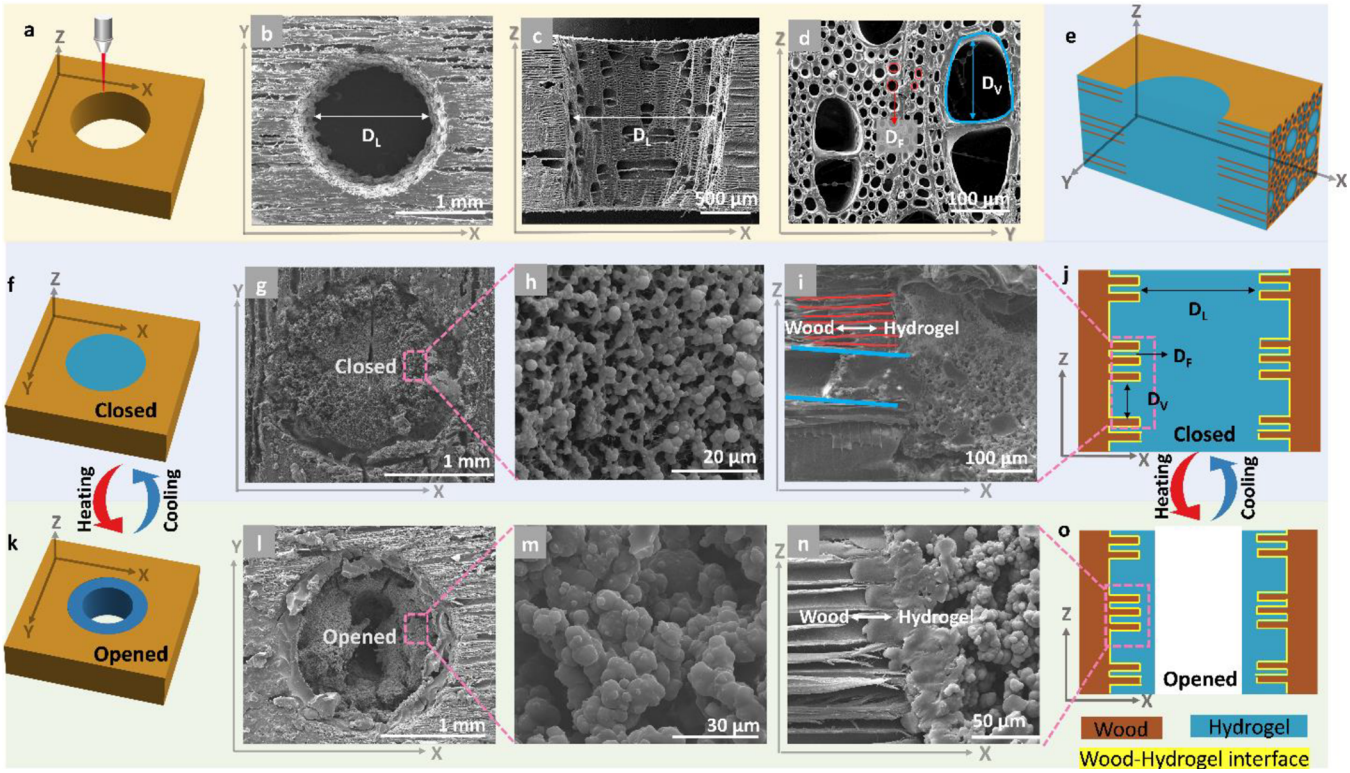

Figure 2. Structure of the wood scaffold and smart gating wood membrane. (a–d) Laser-drilled wood scaffold, (e–j) hydrogel-filled sample in the hydrated state, and (k–o) hydrogel-filled sample in the dehydrated state. (a) 3D scheme of a non-hydrogel-filled wood scaffold after laser drilling. (b) SEM image of the laser-drilled wood scaffold from the X-Y plane. (c) SEM image of the laser-drilled wood scaffold from the X-Z plane. (d) SEM images of the wood scaffold from the Y-Z plane. The wood vessel and fibers are marked with blue and red lines, respectively. Diameter of (D_L) laser drilled pore, (D_V) vessel, and (D_F) fiber. (e, f) 3D scheme of a hydrogel-filled wood scaffold in the hydrated state. (g) SEM image of the hydrogel-filled poplar scaffold in the hydrated state. (h) SEM image of the hydrogel in laser-drilled pores (hydrated state). (i) SEM image showing the interface of the wood hydrogel in its hydrated state. (j) Scheme showing the representation of the wood scaffold, hydrogel, and interface as seen from the X-Z plane (hydrated state). (k) 3D scheme of a hydrogel-filled wood scaffold in the dehydrated state. (l) SEM image of the hydrogel-filled poplar scaffold in its dehydrated state. (m) SEM image of the hydrogel in laser-drilled pores (dehydrated state). (n) SEM image showing the interface of the wood hydrogel in its dehydrated state. (o) Scheme showing the representation of the wood scaffold, hydrogel, and interface as seen from the X-Z plane (dehydrated state).

possesses high strength and stiffness. The unique hierarchical wood structure, composed of microscale hollow cells, makes it an ideal substrate for functional composites in various applications, such as directional water transport,[7] oil/water separation membranes,[8] nanogenerators,[9] and solar steam generation.[10] Additionally, in a previous work, our group successfully formed PNIPAM hydrogels inside the microporous structure of wood.[11] In this work, we further developed

https://doi.org/10.1021/acssuschemeng.2c00111
ACS Sustainable Chem. Eng. 2022, 10, 5517−5525

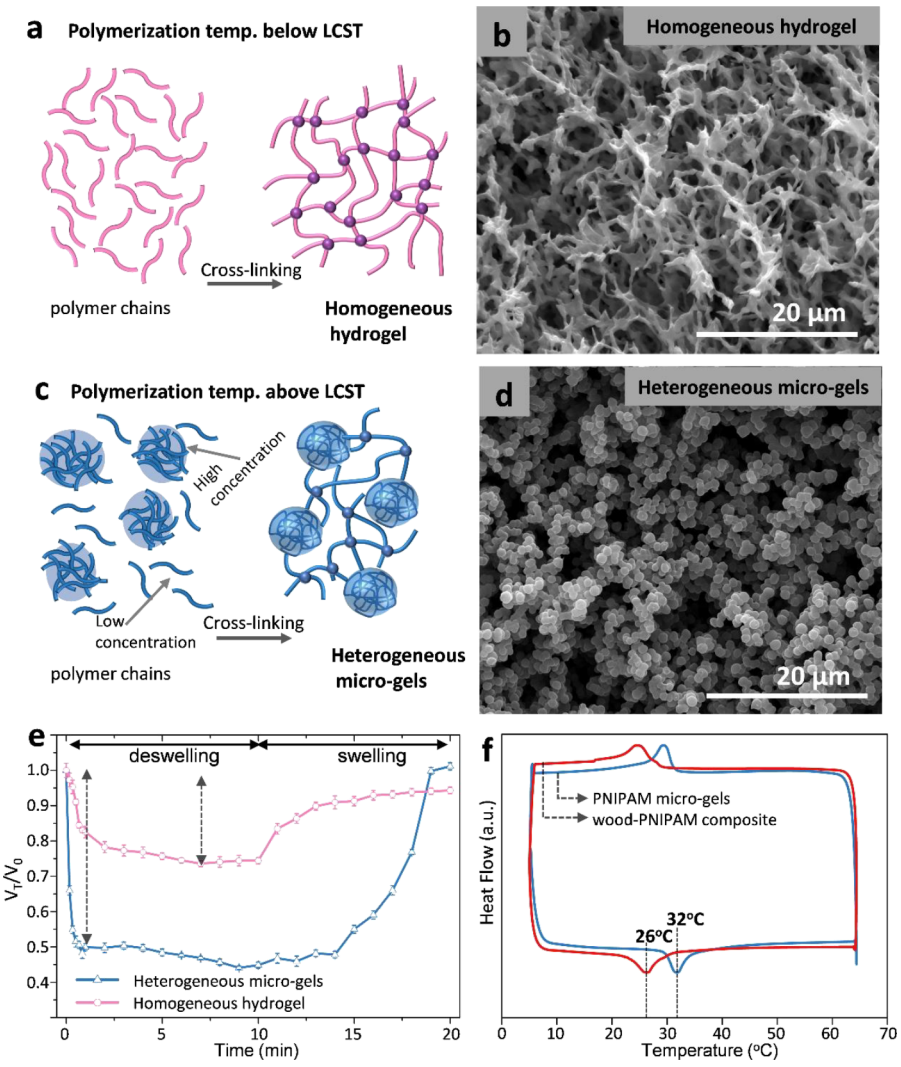

Figure 3. Thermoresponsibility of the PNIPAM hydrogel prepared with different temperatures. Scheme and SEM images of PNIPAM hydrogels obtained by polymerizing (a, b) below LCST and (c, d) above LCST. Schematic diagrams showing the gelation process at two preparation temperatures. Gelation at (a) lower and (c) higher temperatures than the LCST. (e) Dynamic deswelling−swelling behavior of PNIPAM hydrogels obtained with different polymerization temperatures. (f) DSC curves of PNIPAM microgels and wood−hydrogel composites.

the wood−hydrogel composites toward reversible pore actuation for smart gating applications.

RESULTS AND DISCUSSION

Fabrication of Wood-Based Smart Gating Membranes. First, we utilized a laser engraver to drill pore arrays in the tangential plane of poplar wood (Figure 1b, Figures 2a−c, and S1). Afterward, we modified the 3D wood scaffold with methacrylic anhydride (Figure S2). As shown in previous work, the methacrylation treatment increases the dimensional stability and the wood−polymer compatibility.[11] The anhydride reacts with the wood inherent −OH groups, anchoring methacrylate groups, which help forming and stabilizing the hydrogel within the cut-open wood cells. The morphology of the 3D wood scaffold was well preserved (Figure S3) during the methacrylation, and the average weight gain was 5.26 ± 1.35 wt %. The successful grafting of methacrylate groups was further confirmed by the appearance of the modification-specific infrared absorption band at 1718 cm^{-1} (C═O ester) (Figure S4).

The methacrylation of the wood scaffold was then followed by in situ polymerization of thermoresponsive PNIPAM hydrogels (Figure S2). The opaque hydrogel filled the laser-drilled channels but also adjoining parts of the cut-open vessels and fibers (Figure 2e−j). Characteristic peaks in the infrared spectrum of pure PNIPAM at 2964 cm^{-1} ($-CH_3$ asymmetric stretching) and 1639 cm^{-1} (C═O amide) confirmed the presence of PNIPAM inside the wood scaffold (Figure S4). The LCST of PNIPAM, i.e., the temperature at which polymer chains undergo a phase transition from a well-hydrated coil state to a collapsed, hydrophobic globular state, was measured by differential scanning calorimetry (DSC). A clear endothermic transition, associated with the decrease in heat capacity, was recorded for the pure hydrogel and the hydrogel−wood composite samples around the LCST, indicating that the temperature responsive behavior of PNIPAM was successfully maintained in the composites (Figure S5). Thermogravimetric analysis further confirmed the successful preparation of hydrogel−wood composites (Figure S6). The peaks around 345 and 410 °C were related to the degradation of wood and PNIPAM, respectively.

https://doi.org/10.1021/acssuschemeng.2c00111
ACS Sustainable Chem. Eng. 2022, 10, 5517−5525

Parameter and Mechanism Study. We have identified four key requirements for the successful thermoresponsive pore actuation in smart gating wood membranes: (1) a fixed boundary, (2) a thermoresponsive domain, (3) sufficient wood−polymer interfacial interaction, and (4) a suitable microstructure. Following, we comment in detail about their practical implementation.

(1) Fixed boundary. The laser-drilled three-dimensional (3D) wood scaffold acts as a fixed and geometric boundary, ensuring the mechanical stability of the composite. For clarity reasons, we refer to X-Y-Z axes in the following to describe the samples' spatial structure. Laser-drilled pores with a diameter of 1.5 mm distributed equally across the X-Y plane with a distance of 2 mm in the Z-axis direction (Figure 2b). In the X-Z plane, the longitudinally oriented wood vessels and fibers are well-aligned in the horizontal direction (Figure 2c). Looking from the Y-Z plane, the wood vessels and fibers were visible, with lumina diameters between 60 and 100 μm and 5 and 15 μm, respectively (Figure 2d). In short, we obtained a 3D wood scaffold composed of laser-drilled channels (D_L) aligned in the vertical direction and wood cells (vessels D_V and fibers D_F) aligned in the horizontal/longitudinal direction. It is important to note here that laser cutting opened the wood fibers and vessels, resulting in an interconnected tubular structure of drilled channels and cut-open cells.

(2) Thermoresponsive domain. A PNIPAM hydrogel was introduced as the responsive domain by in situ polymerization. Figure 2e shows the schematic representation of the hydrogel-filled wood scaffold. The hydrogel penetrated inside wood vessels and fibers for an average depth of ∼20 μm (Figures 2i and S7). Inspected closely, the in situ formed hydrogel revealed a complex structure. Below LCST, the hydrogel is in its hydrated state and the hydrogel-filled pores were closed (Figure 2f,g). The hydrated hydrogel possessed a sphere-shape morphology (Figure 2h). These hydrogel spheres connect into coils and form a heterogeneous porous structure. A large volume change and fast actuation of the responsive domain are crucial for smart gating membranes as they promote pore opening/closing. We studied the influence of the polymerization temperature on the thermoresponsive behavior of PNIPAM hydrogels.[12] Hydrogels prepared below LCST showed a homogeneous netlike microstructure (Figure 3a,b) because water remained in the polymer network throughout the polymerization reaction.[13] By contrast, when the polymerization temperature was above the LCST of PNIPAM, the polymerization system tended to separate into polymer-rich and polymer-poor regions, as shown in Figure 3c. The polymer-rich regions would lead to the formation of microgel-like regions, while the polymer-poor regions became the links between the microgels in the final heterogeneous network (Figure 3d). The heterogeneous internal microstructure resulted in both a remarkably higher deswelling ratio and more rapid swelling (Figure 3e). The deswelling ratio of the hydrogel prepared above its LCST was two times higher compared to that of the hydrogel prepared below its LCST. The reason might be that the hydrogel prepared above its LCST with the heterogeneous microstructure was composed of numerous microgel particles. The microgel clusters had numerous free ends, which could flex without restriction and consequently deform faster.[14] Consequently, PNIPAM hydrogels were prepared above its LCST to achieve large and fast responsive behavior. In addition, after being introduced into wood scaffolds, the LCST of hydrogel−wood composites (26 °C) was lower than that of the pure hydrogel (32 °C) (Figure 3f). We attributed this to the high density of hydroxyl groups on the wood scaffold, which affected the intermolecular bonding of PNIPAM with water.[15]

(3) Sufficient interfacial interaction. A successful thermoresponsive actuator requires good interfacial interaction between the fixed boundary and responsive domain to avoid the failure at the interface due to hydrogel deformation. When heated above LCST, the hydrogel-filled pore opened from the center (Figure 2k,l). In this dehydrated state, the spherelike hydrogel shrunk into less porous structures (Figure 2m), as heating interrupts the hydrogen bonds between PNIPAM chains and water and intramolecular interactions become dominant. This transition is accompanied by a volume change and release of water from the gel. Importantly, the interface between the wood scaffold and hydrogel remained intact during the swelling and shrinking of the PNIPAM hydrogels (Figures 2i,n,o and S7). This interlocking effect is due to the synergistic effects of a good interfacial interaction and a suitable wood scaffold microstructure. Methacrylation incorporates anchoring points for the polymeric hydrogel and improves the interfacial adhesion between the hydrogel and wood. A comparison of the hydrogel-filled poplar scaffold, which had not been methacrylated, was tested (Figure S8). Although the channels were successfully filled with the hydrogel, upon heating the hydrogel detached from the fixed boundary. This failure proved the importance of a good interface interaction.

(4) Suitable microstructure. The wood scaffold microstructure is another important element enabling pore actuation. Poplar is mainly composed of vessels and fibers with respectively large and narrow lumen diameters. During the in situ polymerization of PNIPAM, the dense hydrogel mass penetrated inside poplar vessels and fibers (Figure 2i). This structure acted as the anchoring point during the dehydration and prevented the failure of the responsive gate. By contrast, spruce wood has tracheids with transition of lumen diameters from earlywood to latewood (Figure S9a,b). After introducing the PNIPAM hydrogel, the hydrogel-filled spruce wood scaffold broke at the interface upon heating and indicated that the microstructure of spruce wood did not favor the pore actuation function (Figure S9c−f).

These results highlight that a reversible thermoresponsive pore actuation could only be achieved thanks to the collective and synergistic influence of the fixed boundary, thermoresponsive domain, interface, and the appropriate microstructure of the selected wood species, i.e., poplar.

Thermoresponsive Pore Actuation. After the successful preparation of the hydrogel−wood composites, we characterized their thermoresponsive actuation properties. The

https://doi.org/10.1021/acssuschemeng.2c00111
ACS Sustainable Chem. Eng. 2022, 10, 5517−5525

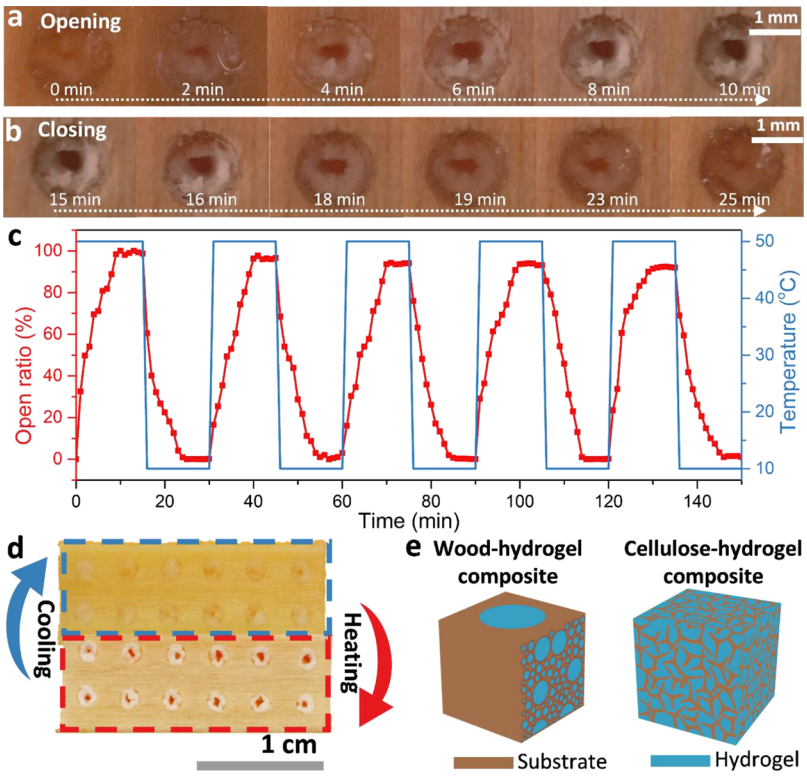

Figure 4. Thermoresponsive pore actuation behavior of the smart gating wood membrane. (a) Light microscopy images showing hydrogel-filled pore opening over time during heating. (b) Light microscopy images showing hydrogel-filled pore closing over time during cooling. (c) Opening ratio of a hydrogel-filled pore during five heating/cooling cycles. (d) Image of the collective thermoresponsive actuation of multiple pores within one wood sample. (e) Illustration showing two different porous structures: wood−hydrogel composite (hierarchical aligned pores) and cellulose−hydrogel composite (disordered irregular pores).

hydrogel-filled pores reversibly closed and opened by subjecting them to a temperature change from 10 to 50 °C. This dynamic response was monitored by light microscopy, and the pore opening ratio was calculated as a function of temperature. After 10 min at 50 °C, the composite revealed a complete pore opening and remained in the opened state without further changes (Figure 4a). Subsequently, by cooling to 10 °C for 10 min, the pores closed and remained in this state (Figure 4b). The pore opening ratios calculated for five heating/cooling cycles indicated a constant thermoresponsive actuation behavior over time (Figure 4c).

Having clarified the actuation dynamics with a pore diameter of 1.5 mm under temperature change, we tested behavior consistency, in terms of reversible pore opening/closing, also for larger samples or different pore diameters. For this purpose, we fabricated wood samples by laser-drilling pores with different diameters D = 0.5, 1, and 2 mm. After introducing PNIPAM, all obtained composites revealed consistent opening and closing actuation behavior during multiple heating/cooling cycles (Figure S10). This adjustability in pore size greatly widens the application potential, since it allows one to adjust pore sizes to sufficiently filter and separate a variety of particles, such as blood cells, pigments, pollens, and sand (Figure S11).[16] Pore actuation simultaneously works for larger samples with multiple pores. A hydrogel−wood composite sample (width in the X-axis = 2 cm; height in the Y-axis = 1 cm) with 12 pores exhibited simultaneous opening/closing behavior under heating/cooling cycles, confirming the feasibility of a collective pore response (Figure 4d).

Our 3D hydrogel-filled wood-based smart gating membrane is significantly different from state-of-the art porous substrates in terms of channel/pore anisotropy, mechanical strength, and potential for scale-up. Although cellulose sponges, for example, would have a similar composition to our wood scaffold (Figure 4e), there are significant differences. First, in our 3D wood scaffold, laser-drilled channels could be fabricated in the direction perpendicular to that of wood vessels/fibers, resulting in high porous anisotropy. After introducing the hydrogel into the 3D wood scaffold, the laser-drilled pores in the vertical direction serve for pore opening/closing and the vessels/fibers in the horizontal direction enhance the interfacial adhesion between the hydrogel and wood scaffold. By contrast, in a cellulose sponge, the pores are homogeneously distributed in all directions, making more difficult to control their hierarchical order.[17] Second, the wood-based smart gating membrane has a higher mechanical robustness than a hydrogel−cellulose sponge composite. The hydrogel−wood composite exhibited a tensile strength of ∼55 MPa, remarkably higher than that of hydrogel−cellulose sponge composites (Figure S12).[18] Finally, the 3D wood scaffold was fabricated on the tangential plane of wood by utilizing a commercial CO_2 laser engraver, making it suitable for large-scale production. By contrast, cellulose sponges are mainly produced by freeze-drying, a procedure for which scale-up is certainly challenging. These advantages of the wood-based smart gating membrane open up the venue for various applications. In this work, we demonstrate their applications in indoor light management and as a water flow manipulator.

https://doi.org/10.1021/acssuschemeng.2c00111
ACS Sustainable Chem. Eng. 2022, 10, 5517−5525

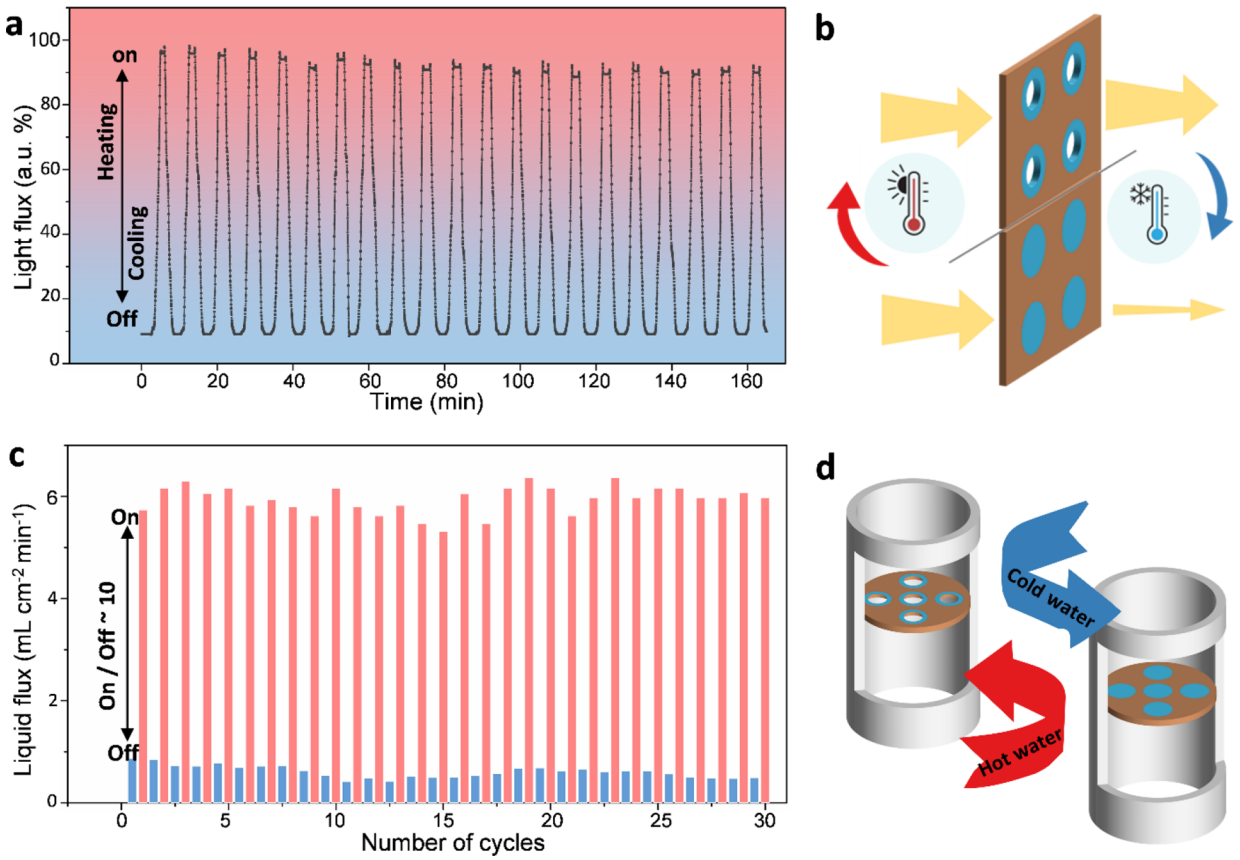

Figure 5. Applications of the smart gating wood membranes. (a) Temperature-controlled light transmission and (b) application as an energy-efficient smart window, which could open and transmit light and air at high temperatures and close at lower ones. (c) Thermoresponsive water permeability of the smart gating membrane and (d) its application for the thermoresponsive water flow manipulator.

Potential Applications of the Smart Gating Wood Membranes. *Indoor Light Management.* Heating, cooling, lighting, and humidification account for more than 40% of energy use in buildings.[19] Passive designs for the control of light and heat can greatly reduce energy consumption and the environmental impact. However, such designs are usually static, which is not ideal for changing (diurnally or seasonally variable) environments. On the other hand, adaptive controllers for light and heat, such as electrochromic and thermochromic designs, are sophisticated and expensive, limiting their applicability. In this work, we tested the light transmission of wood−hydrogel smart gating membranes at 20 and 40 °C (Figure S13a). As shown in Figure 5a, the hydrogel gates closed below LCST. Due to its heterogeneous microstructure, the hydrogel is opaque, and consequently, the light intensity was reduced to ∼10%. As the temperature increased above the LCST, the hydrogel dehydrated and shrunk, and the gates opened and transmittance increased to ∼95%. During the cooling phase, extra water was supplied by exposing samples to water mist to keep the hydrogel moist. The hydrogel hydrated and swelled back to close the gates. This pore opening/closing could be achieved in 20 min. The reversible light transmittance efficiency remained unchanged after 20 heating/cooling cycles, demonstrating as a first proof of the potential stability of the device. Based on these results, we envisage the utilization of wood−hydrogel composites for indoor light management (Figure 5b).

Water Flow Manipulator. Controlled fluid manipulation has become a topic of great interest for applications, e.g., as filters, smart sensors, and microreactors. Compared to conventional methods, thermoresponsive flow manipulators have many advantages, such as simple operation and low energy demand.[2,20] We measured the water permeability of wood−hydrogel composites at 20 and 40 °C (Figures 5c and S13b). A remarkable flux difference was observed when the temperature was increased above LCST. The average flux was 0.6 mL min^{-1} at 20 °C and 5.9 mL min^{-1} at 40 °C (approximately a 10 times change). The gating function of water flux was conserved even after 30 cycles, indicating excellent stability. Although a full on−off gating was not achievable, these results prove the great potential for wood−hydrogel composites as thermoresponsive water flow manipulators (Figure 5d).

CONCLUSIONS

We have established a facile strategy for preparing a wood-based smart gating membrane, by taking advantage of the wood hierarchical porous structure and of PNIPAM hydrogel thermoresponsiveness. With laser drilling, wood fibers and vessels were cut open and the 3D interconnected wood scaffold with well-aligned order, uniform pore size, and superior mechanical strength was employed as the fixed boundary of the smart gating membrane. A thermoresponsive domain was introduced into the wood scaffold by in situ polymerization of PNIPAM hydrogels. Hydrogels prepared above the LCST showed a heterogeneous microstructure with microgel clusters, resulting in a remarkable deswelling ratio and rapid swelling. Moreover, the methacrylation pretreatment and

https://doi.org/10.1021/acssuschemeng.2c00111
ACS Sustainable Chem. Eng. 2022, 10, 5517−5525

a suitable microstructure of the wood scaffold played an important role in promoting the good interfacial strength between the responsive domain and fixed boundary ensuring proper pore actuation. The wood−hydrogel membranes exhibited opening/closing and stable pore actuation under heating/cooling cycles. The rapid response and feasibility of scale-up open the venues for practical applications of this smart gating wood membrane. Since the thermoresponsive behavior of PNIPAM depends on its hydration state, in its current configuration, our smart gating wood membrane requires high relative humidity or moist conditions. Meanwhile, we demonstrated their applications for indoor light management and smart flow manipulation. The smart gating wood membranes exhibited remarkable switching capacity (10 times flux difference), fast response (close/open gates in 10 min), and stable pore actuation.

EXPERIMENTAL SECTION

Fabrication of Wood Membranes. Poplar wood samples were cut with a circular saw into a dimension of 50 × 50 × 1.5 mm^3 (tangential × longitudinal × radial). The wood scaffold with a desired channel pattern was produced with a laser engraver (Trotec, Speedy 300). The wood samples were stored in a controlled climate (20 °C, 65% relative humidity) before treatment and characterization.

Methacrylation of Wood Membranes. Wood samples were first dried at 65 °C for 48 h until a constant mass was obtained. Dried wood samples were placed into a flask under high vacuum for 45 min. In a separate flask, a solution of methacrylic anhydride in dry pyridine was prepared. (methacrylic anhydride/pyridine solution: 0.2 g/mL). This solution was injected into the evacuated flask with the wood samples, heated to 70 °C, and the samples were reacted for 8 h. After reaction completion, the samples were washed in a methanol/water (1:1 v/v) mixture for 24 h. The washing solution was exchanged five times, and the samples were stored in Milli-Q water at 5 °C for further experiments. The washing procedure was followed by drying the samples at 65 °C, and the weight gain was determined.

In Situ Polymerization of the PNIPAM Hydrogel. Hydrogel films were synthesized by dissolving the monomer NIPAM, the crosslinker *N*, *N*′-methylenebis(acrylamide), and the UV-initiator 1-[4-(2-hydroxyethoxy)-phenyl]-2-hydroxy-2-methyl-1-propane-1-one in Milli-Q water. The resulting solution was degassed with nitrogen for 2 min and then put into a refrigerator for 60 min. The liquid was poured intro Petri dishes and placed on top of a heating plate. The polymerization was initiated with an UV-lamp (CAMAG, λ = 366 nm) placed on top. The solution was irradiated for 20 min. PNIPAM hydrogels were prepared with different polymerization temperatures, monomer concentrations, and crosslinking ratios. The detailed recipes are listed in Table S1. After polymerization, hydrogel films were washed with Milli-Q water. The films were switched five times by putting them into a 20 °C and a 45 °C water bath. The films were stored in Milli-Q water at 5 °C.

Wood−Hydrogel Composite Preparation. The methacrylated wood samples were placed into a flask under vacuum for 30 min. Monomer solution was prepared (NIPAM monomer concentration: 2.0 mol/L; crosslinker/monomer = 0.01 mol/mol; initiator/monomer = 0.02 mol/mol).

The monomer solution was injected into the evacuated flask. The wood samples were impregnated in the monomer solution at 65 °C for 1 h with gentle stirring. Then, the monomer-impregnated wood samples were placed on a heating plate at 65 °C and UV-irradiated for 20 min (CAMAG, λ = 366 nm). After polymerization, the composites were washed with Milli-Q water. The composites were switched five times by putting them into a 20 °C and a 45 °C water bath. The samples were stored in Milli-Q water at 5 °C.

Pore Actuation Behavior Measurement. For the heating/cooling of samples, a commercial thermoelectric Peltier plate (TEC1-26308) was used. An external voltage supply was used to control the temperature. The samples were placed on a Peltier plate, and the temperature was set at 50 °C and held for 15 min (heating condition). Then, the temperature of the Peltier plate was changed to 10 °C and held for 15 min (cooling condition). Because the water is necessary for the swelling of the PNIPAM hydrogel, extra water was supplied by spraying water on the samples with a humidifier during the cooling. These heating/cooling cycles were repeated five times, and the pore actuation behavior was recorded on a Leica M165C stereomicroscope coupled to a Basler GigE Vision camera. Images and videos were recorded with a control plugin (PHASE GmbH) for the program ImageJ. The pore diameters were measured. The diameter of the opened pore at 50 °C for 10 min was defined as the maximum r (r_{max}), and the pore opening ratio was defined in eq 1:

$$\text{opening ratio} = \frac{r_t}{r_{max}} \tag{1}$$

where r_t is the diameter of the opening pore at time t. The specimen released and took in water during the heating and cooling process, respectively.

Hydrogel Deswelling−Swelling Ratio Measurement. Hydrogel membranes, having a thickness of 2 mm, were prepared with different recipes. The gels were stabilized at 5 °C for 24 h and then cut into 2 × 2 cm^2. The samples were placed on a glass slide and then mounted on the Peltier plate for heating/cooling. The dynamic deswelling−swelling behavior was recorded on a camera, and the images were analyzed by ImageJ. The deswelling ratio was calculated using eq 2:

$$\text{deswelling ratio} = \frac{V_T}{V_0} \tag{2}$$

where V_0 is the initial surface area of hydrogel membranes, and V_T is the surface area at time t.

Thermoresponsive Light Transmittance Measurement. The thermoresponsive light transmittance test set-up consisted of four parts: photo-resistor, LED lamp, test house, and temperature control chamber. These functional units were assembled together for the thermoresponsive light transmittance measurement. The heating stage (40 °C) and the cooling stage (20 °C) were held for 10 min each. The heating/cooling cycle was repeated 20 times.

Thermoresponsive Water Permeability Measurement. The composite membrane was fixed to a filter holder connected to a water column, and the flux of deionized water was measured by recording the time needed for 10 mL of water to be filtered through the membrane under atmospheric pressure. The permeation of water at 20 and 40 °C was repeated for 30 cycles. The water flux F (mL cm^{-2} min^{-1}) was calculated using eq 3:

$$F = \frac{V}{A \times t} \tag{3}$$

where V (mL) is the volume of deionized water. A = 3.14 cm^2 is the area of the membrane, and t (min) is the time for the water to pass through the membrane.

Characterizations. *SEM.* The surface morphology and chemical composition of wood membranes were studied with a scanning electron microscope (SEM; FEI Quanta 200F, Hillsboro, OR, USA) equipped with energy-dispersive X-ray spectroscopy (EDXS; Ametek-EDAX). Wood samples were coated with a sputter coater (CCU-010, Safematic, Switzerland). A Pt−Pd (80/20) coating of ∼10 nm thickness was applied.

Fourier Transform Infrared Spectra (FT-IR). FT-IR spectra were acquired with a Bruker FT-IR equipped with an ATR module.

Differential Scanning Calorimetry (DSC). The conformational change of the samples at the LCST was determined using a DSC Q2000 (TA instruments). All samples were immersed in Milli-Q water at 15 °C and allowed to reach equilibrium swelling before measurement. Samples of approximately 5 mg were placed into a Tzero hermetic aluminum pan, and the analysis was performed from 10 to 60 °C at a heating rate of 10 °C min^{-1}.

Thermogravimetric Analysis. Thermogravimetric analyses of ∼10 mg of wood specimens were performed using a Q50 TGA (TA

https://doi.org/10.1021/acssuschemeng.2c00111
ACS Sustainable Chem. Eng. 2022, 10, 5517−5525

instruments) at a heating rate of 10 °C min^{-1} in an N_2 atmosphere (60 mL min^{-1} sample purge flow and 40 mL min^{-1} balance purge flow in the 30−1000 °C temperature range).

Tensile Tests. Tensile tests were performed using a universal testing machine (Zwick Roell) equipped with a 10 kN load cell. Ten specimens stored at 20 °C and 65% relative humidity with the dimensions 5 × 50 × 1.5 mm^3 (tangential × longitudinal × radial) were used with 25 mm initial length between two grips and tested in the longitudinal direction. The testing speed was 0.5 mm min^{-1}.

■ ASSOCIATED CONTENT

Supporting Information

The Supporting Information is available free of charge at https://pubs.acs.org/doi/10.1021/acssuschemeng.2c00111.

Laser drilling process; fabrication process; FT-IR spectra; DSC curves; TGA curves; EDS mapping images and spectrum; SEM images of the hydrogel-filled poplar scaffold without methacrylation pretreatment; SEM images of spruce and spruce wood/hydrogel composites; light microscopy images of the pore actuation behavior of different laser-drilling pore diameters; size range of gating membranes; stress−strain curves of tensile tests; light transmission test and fluid permeability test set up; PNIPAM hydrogel preparation recipes and conditions; dynamic and equilibrium deswelling behavior of PNIPAM hydrogels (PDF)

Pore actuation five-cycle measurement (MP4)

■ AUTHOR INFORMATION

Corresponding Author

Ingo Burgert − *Wood Materials Science, Institute for Building Materials, ETH Zürich, Zürich 8093, Switzerland; WoodTec Group, Cellulose & Wood Materials, Empa, Dübendorf 8600, Switzerland;* orcid.org/0000-0003-0028-072X; Email: iburgert@ethz.ch

Authors

Yong Ding − *Wood Materials Science, Institute for Building Materials, ETH Zürich, Zürich 8093, Switzerland; WoodTec Group, Cellulose & Wood Materials, Empa, Dübendorf 8600, Switzerland;* orcid.org/0000-0003-2781-5616

Guido Panzarasa − *Wood Materials Science, Institute for Building Materials, ETH Zürich, Zürich 8093, Switzerland; WoodTec Group, Cellulose & Wood Materials, Empa, Dübendorf 8600, Switzerland;* orcid.org/0000-0003-1044-0491

Sandro Stucki − *Wood Materials Science, Institute for Building Materials, ETH Zürich, Zürich 8093, Switzerland; WoodTec Group, Cellulose & Wood Materials, Empa, Dübendorf 8600, Switzerland*

Tobias Keplinger − *Wood Materials Science, Institute for Building Materials, ETH Zürich, Zürich 8093, Switzerland; WoodTec Group, Cellulose & Wood Materials, Empa, Dübendorf 8600, Switzerland;* orcid.org/0000-0003-0488-6550

Complete contact information is available at: https://pubs.acs.org/10.1021/acssuschemeng.2c00111

Author Contributions

Y.D., G.P., I.B., and T.K. conceived the study; Y.D. and S.S. designed and carried out the experiments and characterizations; Y.D., G.P., I.B., and T.K. co-wrote the manuscript. All authors discussed the results and commented on the manuscript.

Notes

The authors declare no competing financial interest.
All data are available in the manuscript or the supplementary materials.

■ ACKNOWLEDGMENTS

The project was conducted in the framework of the SNF project "Hierarchical cellulose scaffolds for structural and functional gradient materials" (200021_184821/1). We thank the Scientific Center for Optical and Electron Microscopy at ETH Zurich for providing access to their facilities and Thomas Schnider for the wood sample preparation.

■ REFERENCES

(1) Liu, Z.; Wang, W.; Xie, R.; Ju, X. J.; Chu, L. Y. Stimuli-responsive smart gating membranes. *Chem. Soc. Rev.* **2016**, *45*, 460−475.

(2) du, Y.; Cheng, H.; Li, Y. Z.; Wang, B. J.; Mao, Z. P.; Xu, H.; Zhang, L. P.; Zhong, Y.; Yan, X. L.; Sui, X. F. Temperature-responsive cellulose sponge with switchable pore size: Application as a water flow manipulator. *Mater. Lett.* **2018**, *210*, 337−340.

(3) (a) Liu, H. L.; Liu, X. L.; Meng, J. X.; Zhang, P. C.; Yang, G.; Su, B.; Sun, K.; Chen, L.; Han, D.; Wang, S. T.; Jiang, L. Hydrophobic Interaction-Mediated Capture and Release of Cancer Cells on Thermoresponsive Nanostructured Surfaces. *Adv. Mater.* **2013**, *25*, 922−927. (b) Fan, X. X.; Xie, R.; Zhao, Q.; Li, X. Y.; Ju, X. J.; Wang, W.; Liu, Z.; Chu, L. Y. Dual pH-responsive smart gating membranes. *J. Membr. Sci.* **2018**, *555*, 20−29. (c) Liu, H. W.; Zhu, J. J.; Hao, L.; Jiang, Y. L.; van der Bruggen, B.; Sotto, A.; Gao, C. J.; Shen, J. N. Thermo- and pH-responsive graphene oxide membranes with tunable nanochannels for water gating and permeability of small molecules. *J. Membr. Sci.* **2019**, *587*, 117163. (d) Wong, W. S. Y.; Gengenbach, T.; Nguyen, H. T.; Gao, X.; Craig, V. S. J.; Tricoli, A. Dynamically Gas-Phase Switchable Super(de) wetting States by Reversible Amphiphilic Functionalization: A Powerful Approach for Smart Fluid Gating Membranes. *Adv. Funct. Mater.* **2018**, *28*, No. 1704423. (e) Gajda, A. M.; Ulbricht, M. Magnetic Fe3O4 nanoparticle heaters in smart porous membrane valves. *J. Mater. Chem. B* **2014**, *2*, 1317−1326.

(4) (a) Zelitch, I. Stomatal Control. *Annu. Rev. Plant Physiol.* **1969**, *20*, 329−350. (b) Humble, G. D.; Hsiao, T. C. Light-Dependent Influx and Efflux of Potassium of Guard Cells during Stomatal Opening and Closing. *Plant Physiol.* **1970**, *46*, 483−487. (c) Raschke, K. Stomatal Action. *Annu. Rev. Plant Physiol.* **1975**, *26*, 309−340. (d) Park, Y.; Gutierrez, M. P.; Lee, L. P. Reversible Self-Actuated Thermo-Responsive Pore Membrane. *Sci. Rep.* **2016**, *6*, 39402.

(5) Wandera, D.; Wickramasinghe, S. R.; Husson, S. M. Stimuli-responsive membranes. *J. Membr. Sci.* **2010**, *357*, 6−35.

(6) (a) Ke, Y. J.; Zhou, C. Z.; Zhou, Y.; Wang, S. C.; Chan, S. H.; Long, Y. Emerging Thermal-Responsive Materials and Integrated Techniques Targeting the Energy-Efficient Smart Window Application. *Adv. Funct. Mater.* **2018**, *28*, 28. (b) Tokarev, I.; Minko, S. Stimuli-Responsive Porous Hydrogels at Interfaces for Molecular Filtration, Separation, Controlled Release, and Gating in Capsules and Membranes. *Adv. Mater.* **2010**, *22*, 3446−3462. (c) Wang, W.; Tian, X.; Feng, Y.; Cao, B.; Yang, W.; Zhang, L. Thermally on− off switching membranes prepared by pore-filling poly (n-isopropylacrylamide) hydrogels. *Ind. Eng. Chem. Res.* **2010**, *49*, 1684−1690.

(7) Ding, Y.; Tu, K. K.; Burgert, I.; Keplinger, T. Janus wood membranes for autonomous water transport and fog collection. *J. Mater. Chem. A* **2020**, *8*, 22001−22008.

(8) Vidiella del Blanco, M.; Fischer, E. J.; Cabane, E. Underwater Superoleophobic Wood Cross Sections for Efficient Oil/Water Separation. *Adv. Mater. Interfaces* **2017**, *4*, No. 1700584.

(9) Sun, J. G.; Guo, H. Z.; Schädli, G. N.; Tu, K. K.; Schär, S.; Schwarze, F. W. M. R.; Panzarasa, G.; Ribera, J.; Burgert, I. Enhanced

mechanical energy conversion with selectively decayed wood. *Sci. Adv.* **2021**, *7*, No. eabd9138.
(10) Zhu, M.; Li, Y.; Chen, F.; Zhu, X.; Dai, J.; Li, Y.; Yang, Z.; Yan, X.; Song, J.; Wang, Y.; et al. Plasmonic Wood for High-Efficiency Solar Steam Generation. *Adv. Energy Mater.* **2018**, *8*, No. 1701028.
(11) Keplinger, T.; Cabane, E.; Berg, J. K.; Segmehl, J. S.; Bock, P.; Burgert, I. Smart Hierarchical Bio-Based Materials by Formation of Stimuli-Responsive Hydrogels inside the Microporous Structure of Wood. *Adv. Mater. Interfaces* **2016**, *3*, No. 1600233.
(12) Seiffert, S. Origin of nanostructural inhomogeneity in polymer-network gels. *Polym. Chem.* **2017**, *8*, 4472−4487.
(13) (a) Hirokawa, Y.; Okamoto, T.; Kimishima, K.; Jinnai, H.; Koizumi, S.; Aizawa, K.; Hashimoto, T. Sponge-like Heterogeneous Gels: Hierarchical Structures in Poly(N-isopropylacrylamide) Chemical Gels As Observed by Combined Scattering and Confocal Microscopy Method. *Macromolecules* **2008**, *41*, 8210−8219. (b) Seiffert, S. Scattering perspectives on nanostructural inhomogeneity in polymer network gels. *Prog. Polym. Sci.* **2017**, *66*, 1−21.
(14) (a) Ju, X. J.; Chu, L. Y.; Zhu, X. L.; Hu, L.; Song, H.; Chen, W. M. Effects of internal microstructures of poly(N-isopropylacrylamide) hydrogels on thermo-responsive volume phase-transition and controlled-release characteristics. *Smart Mater. Struct.* **2006**, *15*, 1767−1774. (b) Yue, L. L.; Xie, R.; Wei, J.; Ju, X. J.; Wang, W.; Chu, L. Y. Nano-gel containing thermo-responsive microspheres with fast response rate owing to hierarchical phase-transition mechanism. *J. Colloid Interface Sci.* **2012**, *377*, 137−144.
(15) (a) Sun, X.; Tyagi, P.; Agate, S.; Lucia, L.; McCord, M.; Pal, L. Unique thermo-responsivity and tunable optical performance of poly (N-isopropylacrylamide)-cellulose nanocrystal hydrogel films. *Carbohydr. Polym.* **2019**, *208*, 495−503. (b) Sun, X.; Tyagi, P.; Agate, S.; McCord, M. G.; Lucia, L. A.; Pal, L. Highly tunable bioadhesion and optics of 3D printable PNIPAm/cellulose nanofibrils hydrogels. *Carbohydr. Polym.* **2020**, *234*, No. 115898.
(16) Hou, X. Smart Gating Multi-Scale Pore/Channel-Based Membranes. *Adv. Mater.* **2016**, *28*, 7049−7064.
(17) Wang, G.; He, Y.; Wang, H.; Zhang, L. Y.; Yu, Q. Y.; Peng, S. S.; Wu, X. D.; Ren, T. H.; Zeng, Z. X.; Xue, Q. J. A cellulose sponge with robust superhydrophilicity and under-water superoleophobicity for highly effective oil/water separation. *Green Chem.* **2015**, *17*, 3093−3099.
(18) (a) Lu, J. S.; Zhu, W. Y.; Dai, L.; Si, C. L.; Ni, Y. H. Fabrication of thermo- and pH-sensitive cellulose nanofibrils-reinforced hydrogel with biomass nanoparticles. *Carbohydr. Polym.* **2019**, *215*, 289−295. (b) Li, Y. Z.; Zhu, L. Q.; Wang, B. J.; Mao, Z. P.; Xu, H.; Zhong, Y.; Zhang, L. P.; Sui, X. F. Fabrication of Thermoresponsive Polymer-Functionalized Cellulose Sponges: Flexible Porous Materials for Stimuli-Responsive Catalytic Systems. *ACS Appl. Mater. Interfaces* **2018**, *10*, 27831−27839. (c) Zhang, X. F.; Wang, Y. R.; Zhao, J. Q.; Xiao, M. J.; Zhang, W.; Lu, C. H. Mechanically Strong and Thermally Responsive Cellulose Nanofibers/Poly(N-isopropylacrylamide) Composite Aerogels. *ACS Sustainable Chem. Eng.* **2016**, *4*, 4321−4327. (d) Haq, M. A.; Su, Y. L.; Wang, D. J. Mechanical properties of PNIPAM based hydrogels: A review. *Mater. Sci. Eng. C Biomim. Mater. Sens. Syst.* **2017**, *70*, 842−855. (e) Keplinger, T.; Wittel, F. K.; Rüggeberg, M.; Burgert, I. Wood Derived Cellulose Scaffolds-Processing and Mechanics. *Adv. Mater.* **2021**, *33*, No. 2001375.
(19) (a) Mandal, J.; Jia, M.; Overvig, A.; Fu, Y.; Che, E.; Yu, N.; Yang, Y. Porous polymers with switchable optical transmittance for optical and thermal regulation. *Joule* **2019**, *3*, 3088−3099. (b) Jain, R. K.; Taylor, J. E.; Peschiera, G. Assessing eco-feedback interface usage and design to drive energy efficiency in buildings. *Energy Build.* **2012**, *48*, 8−17.
(20) Wang, Y.; Liu, C.; Shi, D.; Dong, L.; Chen, M.; Dong, W. J. C. C. Thermo-responsive membranes fabricated by immobilization of microgels with enhanced gating coefficient and reversible behavior. *Compos. Commun.* **2021**, *27*, No. 100840.

https://doi.org/10.1021/acssuschemeng.2c00111
ACS Sustainable Chem. Eng. 2022, 10, 5517−5525